Report Number: wucse-2009-19

2009

Geodesic grassfire for computing mixed-dimensional skeletons

Lu Liu and Tao Ju

Skeleton descriptors are commonly used to represent, understand and process shapes. While existing methods produce skeletons at a fixed dimension, such as surface or curve skeletons for a 3D object, often times objects are better described using skeleton geometry at a mixture of dimensions. In this paper we present a novel algorithm for computing mixed-dimensional skeletons. Our method is guided by a continuous analogue that extends the classical grassfire erosion. This analogue allows us to identify medial geometry at multiple dimensions, and to formulate a measure that captures how well an object part is described by medial geometry at...
Read complete abstract on page 2.

Geodesic grassfire for computing mixed-dimensional skeletons

Lu Liu and Tao Ju

Complete Abstract:

Skeleton descriptors are commonly used to represent, understand and process shapes. While existing methods produce skeletons at a fixed dimension, such as surface or curve skeletons for a 3D object, often times objects are better described using skeleton geometry at a mixture of dimensions. In this paper we present a novel algorithm for computing mixed-dimensional skeletons. Our method is guided by a continuous analogue that extends the classical grassfire erosion. This analogue allows us to identify medial geometry at multiple dimensions, and to formulate a measure that captures how well an object part is described by medial geometry at a particular dimension. Guided by this analogue, we devise a discrete algorithm that computes a topology-preserving skeleton by iterative thinning. The algorithm is simple to implement, and produces robust skeletons that naturally capture shape components. Under Review

2009-19

Geodesic grassfire for computing mixed-dimensional skeletons

Authors: Lu Liu, Tao Ju

Corresponding Author: taoju@cs.wustl.edu

Abstract: Skeleton descriptors are commonly used to represent, understand and process shapes. While existing methods produce skeletons at a fixed dimension, such as surface or curve skeletons for a 3D object, often times objects are better described using skeleton geometry at a mixture of dimensions. In this paper we present a novel algorithm for computing mixed-dimensional skeletons. Our method is guided by a continuous analogue that extends the classical grassfire erosion. This analogue allows us to identify medial geometry at multiple dimensions, and to formulate a measure that captures how well an object part is described by medial geometry at a particular dimension. Guided by this analogue, we devise a discrete algorithm that computes a topology-preserving skeleton by iterative thinning. The algorithm is simple to implement, and produces robust skeletons that naturally capture shape components.

Notes:
Under review

Type of Report: Other

Geodesic grassfire for computing mixed-dimensional skeletons

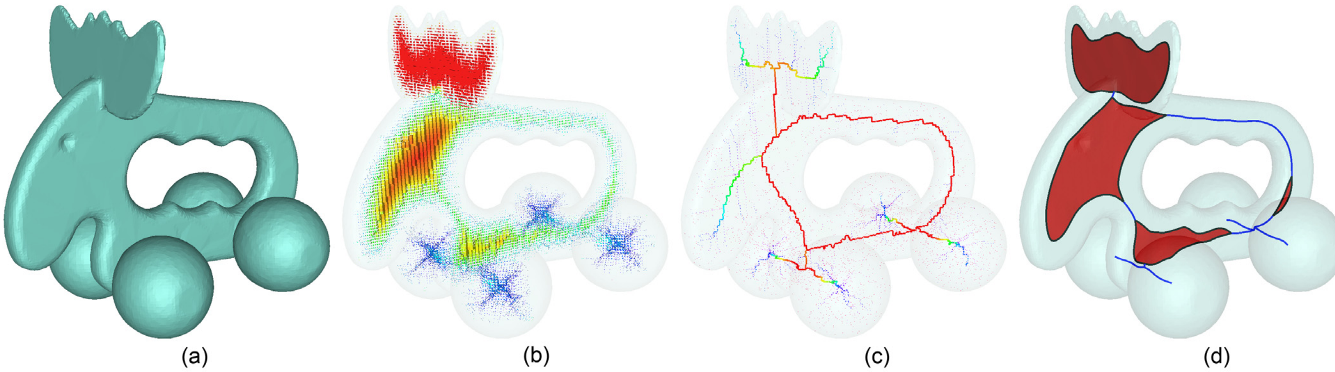

Figure 1: A 3D input model (a), the discrete medial faces (b) and edges (c) computed using our algorithm (redder color indicates where the object shape is more suitable to be depicted by medial surfaces (b) or curves (c)), and the final skeleton (d) (shown with geometric fairing).

Abstract

Skeleton descriptors are commonly used to represent, understand and process shapes. While existing methods produce skeletons at a fixed dimension, such as surface or curve skeletons for a 3D object, often times objects are better described using skeleton geometry at a mixture of dimensions. In this paper we present a novel algorithm for computing mixed-dimensional skeletons. Our method is guided by a continuous analogue that extends the classical grassfire erosion. This analogue allows us to identify medial geometry at multiple dimensions, and to formulate a measure that captures how well an object part is described by medial geometry at a particular dimension. Guided by this analogue, we devise a discrete algorithm that computes a topology-preserving skeleton by iterative thinning. The algorithm is simple to implement, and produces robust skeletons that naturally capture shape components.

1 Introduction

Describing shapes is an important task in graphics and vision. A simple, concise descriptor that captures the essence of an object greatly facilitates computer-based understanding of the object and applications such as matching and segmentation. For this reason, medial descriptors (or skeletons) have been well studied and widely used. These descriptors, at lower dimensions, lie interior to the objects and capture visually prominent shape features such as protrusions. Typically, medial descriptors consist of geometry at a fixed dimension. For example, the medial axes, introduced by Blum [1967], generally consist of $(n-1)$-dimensional manifolds (e.g., surfaces) in an n-dimensional object (e.g., a 3D solid). Curve skeletons of 3D objects, which are important in animation control, lie on an even lower dimension.

Often times, an object can be better described using skeletons at a mixture of dimensions. Consider the toy car example in Figure 1 (a). The head and crown of the car, which are thin and wide, can be well depicted using a medial surface. The back-handle, on the other hand, is much more elongated in one direction, and is better described as a medial curve rather than a thin band of medial surface. For this and many other models that we shall see, a mixed-dimensional skeleton serves as a better descriptor than either a 1D or 2D skeleton alone.

In this paper, we propose computing a skeleton that consists of medial geometry at a mixture of dimensions based on local shape anisotropy. Our algorithm proceeds in two steps. First, we compute medial geometry at all dimensions k for $k < n$. Second, for each k, we identify parts of the k-dimensional medial geometry that describe the shape well.

Our algorithm is guided by a continuous, conceptual analogue that we refer to as *geodesic grassfire* (Section 3). This analogue extends Blum's grassfire analogy [Blum 1967], which defines the medial axes, to identify medial geometry at lower dimensions. In addition, the arrival times of the geodesic grassfire front offer an intuitive way to measure how well an object part is described by medial geometry at a particular dimension. Guided by this conceptual analogue, we develop a simple, practical algorithm that extracts a discrete mixed-dimensional skeleton by iterative thinning (Section 4). During the algorithm, discrete medial elements and their measures are computed, as shown in Figure 1 (b,c) for the toy car. Note that medial faces or edges with high measures lie in regions that, intuitively, can be described well by medial surfaces or curves. These elements are then combined to form the final skeleton, as shown in Figure 1 (d).

Contributions In the context of previous work on extracting medial shape descriptors, we make the following contributions:

- We formulate geodesic grassfire, a natural extension of the classical grassfire erosion that defines medial geometry at various dimensions. We show that the arrival times of the fire front intuitively capture how well a object part is represented by medial geometry at a particular dimension.
- We present a discrete algorithm for computing mixed-dimensional skeletons based on iterative thinning. The algorithm is very simple to implement, and produces skeletons that capture well the shape components of 3D models.

2 Previous works

There has been significant amount of work on defining, computing and pruning skeletons. Note that most of these methods are specific to the dimension of the object and/or the dimension of the skeleton. We will briefly review some representative works, while referring readers to excellent survey articles and books such as [Shaked and Bruckstein 1998; Cornea and Min 2007; Siddiqi and Pizer 2008] for extensive discussions.

Defining skeletons Since its introduction by Blum [1967], the medial axes (MA) has become an important descriptor due to its ability in capturing intuitive shape features. The MA is generally $(n-1)$-dimensional within an n-dimensional object, while degenerating to lower-dimensional structures in singular cases (e.g., the MA of a 2D circle is a point). Pizer et al. [2003] reviewed and compared a number of alternative, multi-scale definitions to MA designed to overcome its instability to boundary irregularity.

Unlike MA, there is much less consensus in how medial descriptors at lower dimensions should be defined, and existing definitions are scarce. Dey and Sun [2006] proposed one of the first definitions of the curve skeleton of a 3D object, as the singular points of a medial geodesic function (MGF) on the MA. More recently, Tagliasacchi et al. [2009] defines the curve skeleton of a set of 3D oriented point samples as its rotational symmetric axis (ROSA) in a variational sense. Note that, like [Dey and Sun 2006], the medial curves resulted from our extended grassfire formulation can also be considered as the singular points of a function on the MA surface, where the function is the arrival time of the geodesic grassfire front. In comparison, our formulation is more general and constructs k-dimensional medial geometry in an n-dimensional object for all $k < n$, including the MA (when $k = n-1$).

Computing skeletons Numerous methods have been proposed to compute or approximate the MA [Siddiqi and Pizer 2008]. Broadly speaking, these methods fall in two classes based on their representations of the MA. *Geometric* methods yield explicit geometric representations, such as piece-wise linear curves and surfaces. Examples are methods that compute the MA of a polyhedral model [Sherbrooke et al. 1996; Culver et al. 1999] or approximate the MA as a sub-set of Voroncoi facets induced by a point sampling of the object boundary [Amenta et al. 2001; Dey and Zhao 2003]. On the other hand, *digital* methods represent the object and the MA as a collection of lattice points (e.g., 2D pixels or 3D voxels) based on digital topology [Rosenfeld 1979]. These methods typically involve a thinning procedure [Lam et al. 1992] guided by a distance function [Borgefors et al. 1999], a vector field [Siddiqi et al. 2002], or local feature criteria [Tsao and Fu 1981; Bertrand 1995; Ju et al. 2007].

Algorithms for computing curve skeletons of 3D objects similarly fall into geometric and digital categories [Cornea and Min 2007]. Examples of geometric methods include eroding a medial surface [Dey and Sun 2006], computing the Reeb graph [Pascucci et al. 2007], decomposing the object into parts [Katz and Tal 2003], surface inflation [Sharf et al. 2007], or mesh contraction [Au et al. 2008]. A digital curve skeleton can be computed by thinning from a surface skeleton [Svensson et al. 2002; Ju et al. 2007], or guided by a force field [Chuang et al. 2000; Brunner and Brunnett 2008].

In comparison, geometric methods produce skeletons with explicit connectivity and dimension that makes them convenient for recognition and processing, while digital approaches are often simpler to implement and can more easily enforce topology preservation by thinning. Our algorithm for computing the mixed-dimensional skeletons can be considered as a hybrid approach, in that we perform topology-preserving thinning on an explicit geometric structure (e.g., a cell complex).

There are very few algorithms that compute skeletons with both curve and surface elements. Goswami et al. [2006] extracts the unstable manifold of index 2 and 1 saddle points in the Euclidean distance function, which are respectively 1 and 2 dimensional. While the dimension of these manifolds is determined by local shape properties (e.g., whether the cross-section is near-circular), the dimension of our skeleton elements are chosen by a salience measure that reflects global shape property (e.g., anisotropic elongations).

Pruning skeletons While being an intuitive shape descriptor, the MA is known for its instability to small boundary changes. A variety of salience (or significance, importance, etc.) measures have been proposed for identifying and pruning unstable portions of the MA, in 2D [Shaked and Bruckstein 1998] and 3D [Sud et al. 2005], which can be classified into local or global ones [Reniers et al. 2008; Siddiqi and Pizer 2008]. *Local* measures rate a MA point by surface geometry in its immediate neighborhood, such as the angle formed by the MA point and its two closest surface points [Blum 1967; Dimitrov et al. 2003; Sud et al. 2005] or the distance between the two surface points [Amenta et al. 2001; Dey and Zhao 2002]. While reflecting stability, local measures cannot capture global shape properties such as anisotropy. For example, a point on the crown of the toy car in Figure 1 would have a same (high) local measure as a point on the back-handle of the toy, even though the back-handle exhibits a much greater one-dimensional elongation.

On the other hand, *global* measures capture shape properties in a larger region. Notable examples of 2D global measures are the Maximum Erosion Thickness (MET), which approximates the area of the 2D shape eroded in response to the loss of a skeleton branch [Shaked and Bruckstein 1998], and the Feature-distance [Ogniewicz and Kübler 1995], which expresses the length of the shortest curve on the shape boundary between the closest boundary points to the MA point. One of these 2D measures, the Feature-Distance (FD), has been extended to evaluate 3D surface skeletons using lengths of geodesic curves on surfaces [Dey and Sun 2006; Reniers et al. 2008], and even further to evaluate 3D curve skeletons using approximated areas of geodesic patches [Reniers et al. 2008]. However, as we shall compare in Section 5, the FD measure tends to be high in regions that are further away from the border of the skeleton. In contrast, our salience measure (part of which extends the MET measure) captures more intrinsic shape properties. In addition, our formulation is generally applicable to objects and their medial geometry in any dimensions.

3 Geodesic grassfire

To compute a mixed-dimensional skeleton, our algorithm involves computing medial geometry at various dimensions and identifying portions of medial geometry at each dimension that is suitable for shape description. We shall first describe a conceptual, continuous analogue that guides our algorithm design. We will then present the discrete algorithm in the next section.

Our continuous analogy extends the grassfire analogy that Blum used to described the medial axes (MA). In the grassfire analogy, the object is continuously eroded from its boundary at a uniform speed, as if a grassfire is propagating on a field. The erosion stops when the grassfire fronts meet and quench, resulting in a thin structure – the MA. To construct medial geometry at lower dimensions than that of MA, we shall extend Blum's grassfire onto manifolds of low dimensions. We will first describe the formulation of the extended grassfire and the resulting medial geometry. We will then derive a salience measure that, given medial geometry at a particular dimension, identifies the parts that are most suitable for describing the local shape. Note that our discussion in this section is intended to remain at a conceptual level, for the purpose of motivating our discrete algorithm in the next section.

3.1 Formulation

Consider a continuous erosion of an n-dimensional object by a fire that propagates geodesically on *manifolds* from their boundaries at a uniform speed. When the fire fronts on a k-manifold ($k \leq n$) meet and quench, the object is locally eroded to a thin, $(k-1)$-manifold, which is subject to further erosion. The erosion process terminates

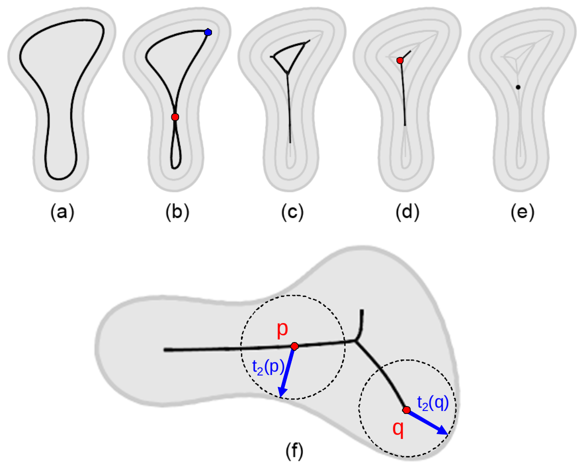

Figure 2: Illustration of geodesic grassfire on a 2D shape.

when the remainder of the object consists only of manifolds without boundaries.

We illustrate this *geodesic grassfire* on a 2D object in Figure 2. As in Blum's grassfire, erosion begins on the boundary of the object, which is a 2-manifold. As the fire fronts meet (in (b)), the object is locally eroded to a thin curve, which is a 1-manifold (e.g., red and blue points in (b)). The erosion on the curve starts as soon as the 2D fire reaches a curve end-point (e.g., blue point in (b)), and the fire propagates along the curve at a same uniform speed (c). A fire front on the curve (e.g., the top left branch) is annihilated when it comes to a junction (e.g., red point in (d)), as the curve end-point disappears. The erosion terminates when either the fire fronts on the curve meet and quench at a point (as in (e)), which is a 0-manifold, or when the remaining curve forms closed rings, which are boundary-less 1-manifolds.

Similarly, geodesic grassfire on a 3D object begins on the boundary of the object (a 3-manifold). The quench sites of the fire front form a surface (a 2-manifold), and erosion starts from the boundary of this surface as soon as the 3D fire reaches there. The quench sites of this surface fire form a curve (a 1-manifold), which is in turn eroded from its end points when the surface fire reaches there. The erosion terminates when the object is eroded to a point, a set of closed rings, or a set of hollow shells (2-manifolds without boundary).

The recursive nature of geodesic grassfire leads to a recursive definition of medial geometry. The k-dimensional medial geometry of an n-dimensional object ($k \leq n$) is the k-manifold formed during geodesic grassfire by fire quenching on $(k+1)$-manifolds. By construction, the medial axes (MA) is the $(n-1)$-dimensional medial geometry, whereas lower-dimensional medial geometry are subsets of the MA. Note that, since the erosion by geodesic grassfire is topology-preserving, medial geometry at some dimensions may not exist for some shapes by our definition. For example, the medial point does not exist for a 2D annulus or a high-genus 3D solid.

3.2 Medial salience

Medial geometry at different dimensions may be good at describing different types of shapes. For example, while a medial surface can describe well a plate-like object in 3D, a medial curve can capture the essence of a tube-like object. Intuitively, a k-dimensional medial geometry is suitable for representing a shape that has a prominent elongation along a k-manifold, a property that we refer to as a *k-anisotropy*. For example, a long tube has a strong 1-anisotropy as its dominant elongation is along a 1D curve, while a wide plate has a strong 2-anisotropy as its primary elongation is isotropic on a 2D surface. To evaluate the "suitability" of medial geometry for shape description, we will measure, at each point on a k-dimensional medial geometry, the strength of k-anisotropy in the local shape.

Here we show that shape anisotropy is well captured by the *difference* in arrival times of the fire fronts along manifolds of different dimensions. Take a 2D object, for example, and consider a point p on the medial curve (Figure 2 (f)). The time at which the fire front from the object boundary reaches p, denoted as $t_2(p)$ (2 means the fire front comes from a 2-manifold), measures the shortest distance from p to the object boundary, or the *maximum* isotropic elongation of the shape centered at p. Since p lies on the medial curve, it will be later reached by the fire front along the curve at some time $t_1(p) \geq t_2(p)$. Note that $t_1(p)$ is the sum of two terms, the geodesic distance from p to some end-point of the medial curve q, and $t_2(q)$. This sum measures the elongation of the shape along the medial curve segment $[p,q]$. In fact, q is chosen by erosion such that $t_1(p)$ measures (half of) the *maximum* elongation of the shape along *any* medial curve segments centered at p. As a result, the larger the time $t_1(p)$ in comparison to $t_2(p)$, the more the shape is elongated along a 1D curve than in other directions at p, and hence there is a stronger 1-anisotropy at p.

We can measure 2- and 1-anisotropy similarly on the medial surfaces and curves of a 3D object. Consider a point p on the medial surface. The arrival time of the fire front from the object boundary, $t_3(p)$, measures the maximum isotropic elongation at p, while the arrival time of the surface fire front, $t_2(p)$ ($t_2(p) \geq t_3(p)$), measures the maximum isotropic elongation of the shape *along* the medial surface. A larger difference between $t_2(p)$ and $t_3(p)$ reflects a more pronounced "side-ways" elongation of the shape along a 2-manifold at p, and hence a stronger 2-anisotropy. Similarly, 1-anisotropy at a point p on the medial curve can be measured by comparing the arrival time of the surface fire front, $t_2(p)$, with the arrival time of the curve fire front, $t_1(p)$ ($t_1(p) \geq t_2(p)$).

Based on these observations, we formulate a unified *salience* measure for any k-dimensional medial geometry in an n-dimensional object ($k \leq n$), assessing its suitability for shape description. The salience at a point p consists of two terms, which capture the absolute and relative strength of k-anisotropy of the local shape,

$$A_k(p) = t_k(p) - t_{k+1}(p), \text{ and } R_k(p) = 1 - \frac{t_{k+1}(p)}{t_k(p)} \quad (1)$$

where $t_k(p) \geq t_{k+1}(p)$ are the arrival times of the fire fronts along the k- and $(k+1)$-dimensional medial geometry. Note that some points on the medial geometry may not be reached by the grassfire when the object has a non-trivial topology (e.g., consider a point on a medial curve that forms a closed ring). For these points, $t_k(p)$ would be infinity, and both salience terms are maximized. Intuitively, the object has infinite k-anisotropy there as the elongation can "wrap around".

Interestingly, in 2D, the first term $A_1(p)$ is identical to the well-known Maximum Erosion Thickness (MET) [Shaked and Bruckstein 1998] for measuring the significance on a MA curve. The MET is low on parts of the MA that respond to small boundary perturbations, which can be explained using our formulation since small bumps on the boundary only introduce small amounts of absolute variation in how much the local shape elongates in different directions. Our formulation further extends MET to medial geometry in higher dimensions, and evaluates high for medial geometry parts corresponding to larger, more stable shape features. On the other hand, the second term $R_k(p)$ is scale-independent and evaluates high for medial geometry that lies in "sharply" anisotropic

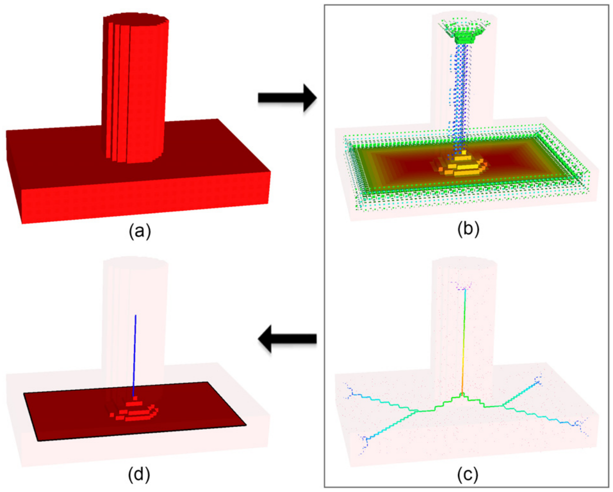

Figure 3: Algorithm flow: given a discrete object represented as a cell complex (a), we first compute medial 2-cells (b) and 1-cells (c) with salience measures using iterative thinning, and then extract, in a second thinning pass, a topology-preserving skeleton containing salient medial curves (blue) and surfaces (red) (d).

parts, such as a flat plate ($k = 2$) or thin tube ($k = 1$), even if their sizes may be small. As a result, we consider a medial geometry to be salient if both terms are high (i.e., describing large and sharp anisotropy).

4 The discrete algorithm

Guided by the our formulation of geodesic grassfire, we now present an algorithm for extracting a discrete skeleton containing salient medial geometry at various dimensions. The algorithm proceeds in two steps. First, we introduce an iterative thinning procedure on a discrete object representation that mimics the continuous erosion process by the geodesic grassfire. Applying thinning on a object (e.g., Figure 3 (a)) results in a set of discrete medial elements each with salience measures (Figure 3 (b,c)). Next, given a user-specified salience threshold, we compute a skeleton containing salient medial elements that additionally preserves the topology of the original object (Figure 3 (d)).

The propagation of geodesic grassfire requires identifying manifolds at different dimensions and their boundaries. As a result, we represent a solid object discretely as a *cell complex*, which consists of geometric elements (cells) at various dimensions. As we shall see, cell complexes admit a simple thinning procedure that closely resembles geodesic grassfire. Using this procedure, discrete medial cells and their salience measures can be similarly defined as in the continuous analogue.

4.1 Cell complexes

A cell complex is a closed set of k-cells, each homotopy equivalent to an open ball in k-dimensions. For example, a point is a 0-cell, an edge without its end points is a 1-cell, and a triangle without its border is a 2-cell. By definition, if a cell δ (e.g., a triangle) is in a cell complex, all cells on the boundary of δ (e.g., corner points and edges) are also in the same complex. A 2D example of a cell complex is shown in Figure 4 (a). A cell complex can be created from other object representations either by triangulating the object interior, or by first voxelizing the model on a grid and constructing cells from grid elements [Zhou et al. 2007]. While the execution of our algorithm is not limited by the type or dimension of the cells, a cell complex with uniform and isotropic cells is preferred for simulating uniform-speed erosion (discussed next).

A manifold and its open boundary can be easily identified on a cell complex. First, let us define an *isolated* cell as one that does not lie on the boundary of any other higher-dimensional cells in the complex (that is, it is "thin"). Furthermore, if a k-cell borders *exactly one* $(k+1)$-cell, the former is called a *witness* cell while the latter is called a *simple* cell. In the example of Figure 4 (b), the edge γ is an isolated edge, while edge σ is a witness edge that borders a simple quad δ. Note that a simple cell is necessarily isolated. Intuitively, a k-manifold consists of isolated k-cells, and the boundary of the manifold consists of witness $(k-1)$-cells.

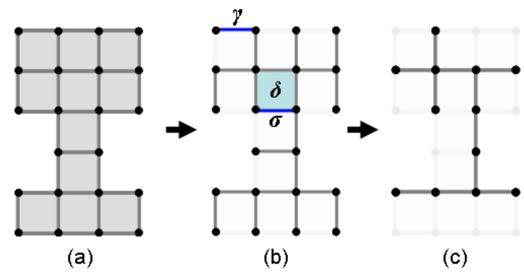

Figure 4: Two iterations of thinning (b,c) on a cell complex (a).

4.2 Computing medial cells and salience

Recall that geodesic grassfire erodes an object from all manifold boundaries simultaneously at a uniform speed. The following iterative thinning procedure mimics this process on a cell complex:

Geodesic grassfire thinning: *At each iteration, identify all simple cells, then remove, in parallel, each identified cell with a witness cell on its boundary.*

Like geodesic grassfire, this thinning erodes a cell complex simultaneously from all its manifold boundaries. The combined removal of simple and witness cells guarantees that the remaining cells after each iteration form a valid cell complex that maintains the topology of the original complex – just like the grassfire erosion. To explain this, we first note that removal of a single pair of simple and witness cells is a *simplicial collapse* [Matveev 2003], which preserves the homotopy and validity of the cell complex. Next, the remaining pairs of simple and witness cells after the removal of one pair are still simple and witness cells. Hence simultaneous removal of all pairs will not jeopardize the topology or validity of the complex. Figure 4 (b,c) illustrates two iterations of thinning in 2D. Note that if multiple witness cells exist on the boundary of a simple cell, an arbitrary one is selected to remove.

Using the thinning procedure, we can define medial geometry and formulate medial salience similarly to geodesic grassfire. The k-dimensional medial geometry ($k < n$) is the k-manifold formed during thinning, which consists of all k-cells in the original cell complex that become isolated at some thinning iteration, referred to as *medial* cells. The salience at a medial k-cell δ can be similarly defined as in Equation 1:

$$A(\delta) = I_{sim}(\delta) - I_{iso}(\delta), \quad \text{and} \quad R(\delta) = 1 - \frac{I_{iso}(\delta)}{I_{sim}(\delta)} \qquad (2)$$

Here, I_{iso} and I_{sim} are respectively the number of iterations after which the cell δ becomes isolated or gets removed as a simple cell, indicating the arrival times of the thinning fronts along the $(k+1)$-manifold and k-manifold. Note that $I_{sim}(\delta) > I_{iso}(\delta)$.

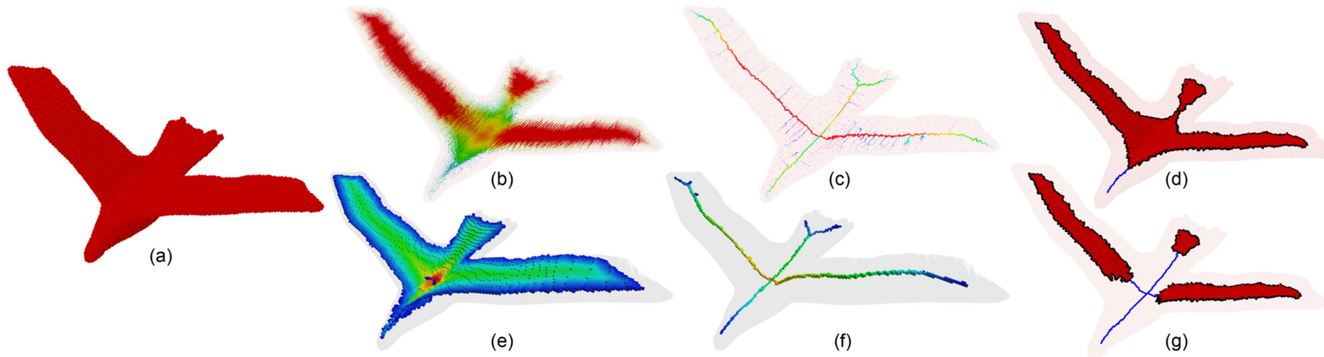

Figure 5: Comparing our salience measures on medial faces (b) and edges (c) with the extended FD measure in [Reniers et al. 2008] on surface (e) and curve (f) skeletons. Skeletons computed using our method at low (0.5) and high (0.7) salience thresholds ε_R^2 are shown in (d,g)

Figure 3 (b,c) visualizes the medial faces and edges with their salience for an input cell complex (a). In this and other figures, the salience is visualized as follows: cells are colored by their $R(\delta)$ values (the redder the higher), while cells with small $A(\delta)$ are shrunk in size. Observe that, due to its scale-dependent formulation, the $A(\delta)$ term (i.e., extension of 2D MET [Shaked and Bruckstein 1998]) is high in regions that are "deeper" into the object, even if the regions do not exhibit a "sharp" feature, such as the column and the diagonal sheets at the edge of the box in (b) and the diagonal curves in the box in (c). On the other hand, the $R(\delta)$ term reflects the "sharpness" of the feature and is low (e.g., in green or blue color) in those regions. The combination of the two measures identify features that are both sharp and at a larger scale, which we next use for computing the skeleton.

4.3 Computing a skeleton

A collection of medial cells at various dimensions with high salience can capture the various types of shape anisotropy. However, a connected skeleton is often desired for practical applications, and some applications further require that the skeleton preserves the topology of the object. Furthermore, for more compact representation, the skeleton should consist of fewer, larger pieces.

To compute a clean, topology-preserving skeleton, we proceed as follows. Given a user-specified salience threshold (for both A, R terms), we identify the set of medial k-cells with high salience at each dimension, and obtain a subset that forms connected components whose sizes are greater than a user-provided number s^k. Next, we re-run the thinning procedure in the previous step, this time preserving the identified set of salient cells. Since thinning is topology-preserving, the remainder after thinning maintains the same topology as the original object. A 2D skeleton computed this way is shown in Figure 3 (d).

Memory-efficient implementation Straight-forward implementation of our algorithm may not be able to handle models at high resolutions ($> 256^3$ voxels), which consume a prohibitive amount of space when represented as a cell complex with uniform cells. To address this issue, both thinning passes in our algorithm are implemented on an adaptive octree grid where only the layer of cells at the current thinning front as well as salient medial cells are maintained at the finest resolution. Octree cells are dynamically collapsed and refined as the thinning proceeds inward.

5 Comparisons and examples

Here we demonstrate our method on a suite of 3D models. All models are constructed from triangular meshes by first converting a mesh into a binary volume [Ju 2004] followed by conversion into a cell complex. Note that the computation of medial cells and their salience is completely parameter-free. Computing the final skeleton is controlled by thresholds $\varepsilon_A^k, \varepsilon_R^k$ of the two salience terms for medial k-cells, and the size of minimum component s^k. Unless otherwise stated, we use $\varepsilon_A^k = 0.05L, \varepsilon_R^k = 0.5, s^k = (0.05L)^k$ for both $k = 1, 2$ in all our examples, where L is the dimension of the bounding box. The test is performed on a PC with 2GB of main memory and 2.2GHz CPU, and time and memory consumption is reported in Figure 9.

We first compare, in Figure 5, our salience measures with those of [Reniers et al. 2008], which extends the 2D Feature-Distance (FD) measure. As observed in (e,f), the FD measures tend to favor regions on the skeleton that are further away from the skeleton boundary. In contrast, our salience measure, particularly the $R(\delta)$ term (e.g., the color), captures well the object parts that have strong anisotropic elongations in two dimensions (e.g., the wings and the tail) or one dimension (e.g., the wings, head, and tail), as seen in (b,c). Using a higher threshold of $R(\delta)$, we are able to obtain a skeleton as in (g) that semantically separates the bird into parts that would not be possible using the FD measures.

We next examine the stability of our salience measures and skeleton under a noisy setting. In Figure 6, we compare the result on a hand model (a) and a synthetically damaged model (e) by applying two iterations of thinning on (a) during which pairs of simple and witness cells are randomly removed. Observe that although the smoothness of the medial cells are affected, due to the nature of thinning, the salience measures are not significantly affected, and the combination of the two salience terms yield skeletons with very similar structures (d,h).

Our discrete thinning algorithm is guided by a continuous analogue. Ideally, the result of our algorithm would converge to that of the continuous analogue as the size of the discrete cells become infinitesimal. Although we do not have any formal proof, we did observe in all our examples, such as that in Figure 7, that the skeleton computed using our method on the same model under the same set of parameters visually converges to a smooth limit as the resolution of the cell complex increases.

Finally, we show a gallery of models and our computed skeletons in Figure 1 and 8. For visual appeal, the skeletons in these examples are smoothed geometrically. Observe that our skeletons naturally capture the varying shape anisotropy on these models using skeleton geometry at different dimensions.

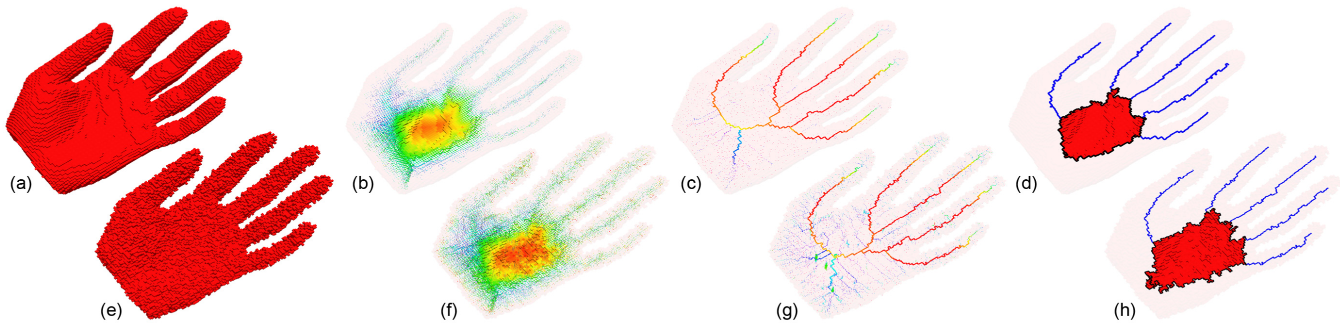

Figure 6: Salience measures and the resulting skeleton of an original model (top row) and one with synthetically added noise (bottom row).

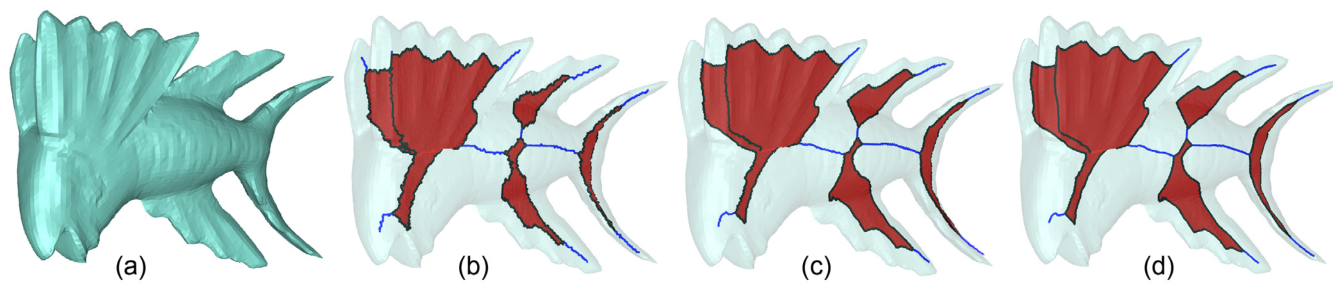

Figure 7: Skeletons computed for a fish model represented by cell complexes on grid resolutions 256^3 (b), 512^3 (c), and 1024^3 (d).

6 Conclusion and discussion

We have presented a novel approach for computing skeleton descriptors that consist of medial geometry at a mixture of dimensions. The *k*-dimensional medial geometry depicts object parts with a strong anisotropic elongation in *k* dimensions. Our algorithm is guided by a continuous analogue that extends the grassfire erosion of medial axes to construct medial geometry at lower dimensions, which additionally offers an intuitive salience measure that captures shape anisotropy. We present a discrete thinning algorithm on cell complexes that mimics the continuous erosion, and extracts the final skeleton as the collection of discrete, salient medial elements.

Limitations and future works Our thinning algorithm relies on the isotropy and uniformity of the cells in the cell complex to simulate a uniform-speed erosion. The use of non-uniform cells would not result in skeletons that lie medial to or reflect the intrinsic anisotropy of the shape. We will investigate means to alleviate the problem, possibly by varying the speed of thinning based on local cell sizes and anisotropy. Other interesting venues for future research include investigating theoretical properties of the geodesic grassfire and its resulting medial geometry, and GPU-accelerated thinning that harvests its highly parallel nature.

References

AMENTA, N., CHOI, S., AND KOLLURI, R. K. 2001. The power crust. In *SMA '01: Proceedings of the sixth ACM symposium on Solid modeling and applications*, 249–266.

AU, O. K.-C., TAI, C.-L., CHU, H.-K., COHEN-OR, D., AND LEE, T.-Y. 2008. Skeleton extraction by mesh contraction. *ACM Transactions on Graphics 27*, 3.

BERTRAND, G. 1995. A parallel thinning algorithm for medial surfaces. *Pattern Recogn. Lett. 16*, 9, 979–986.

BLUM, H. 1967. A transformation for extracting new descriptors of form. *Models for the Perception of Speech and Visual Form*, 362–80.

BORGEFORS, G., NYSTRÖM, I., AND SANNITI DI BAJA, G. 1999. Computing skeletons in three dimensions. *Pattern Recognition 32*, 7, 1225–1236.

BRUNNER, D., AND BRUNNETT, G. 2008. Fast force field approximation and its application to skeletonization of discrete 3D objects. *Computer Graphics forum journal 27*, 2, 261–270.

CHUANG, J.-H., TSAI, C.-H., AND KO, M.-C. 2000. Skeletonization of three-dimensional object using generalized potential field. *IEEE Trans. Pattern Anal. Mach. Intell. 22*, 11, 1241–1251.

CORNEA, N. D., AND MIN, P. 2007. Curve-skeleton properties, applications, and algorithms. *IEEE Transactions on Visualization and Computer Graphics 13*, 3, 530–548. Member-Silver,, Deborah.

CULVER, T., KEYSER, J., AND MANOCHA, D. 1999. Accurate computation of the medial axis of a polyhedron. In *SMA '99: Proceedings of the fifth ACM symposium on Solid modeling and applications*, ACM, New York, NY, USA, 179–190.

DEY, T. K., AND SUN, J. 2006. Defining and computing curve-skeletons with medial geodesic function. In *SGP '06: Proceedings of the fourth Eurographics symposium on Geometry processing*, Eurographics Association, Aire-la-Ville, Switzerland, Switzerland, 143–152.

DEY, T. K., AND ZHAO, W. 2002. Approximate medial axis as a voronoi subcomplex. In *SMA '02: Proceedings of the seventh ACM symposium on Solid modeling and applications*, 356–366.

DEY, T. K., AND ZHAO, W. 2003. Approximating the medial axis from the voronoi diagram with a convergence guarantee. *Algorithmica 38*, 1, 179–200.

DIMITROV, P., DAMON, J. N., AND SIDDIQI, K. 2003. Flux invariants for shape. In *In International Conference on Computer Vision and Pattern Recognition*, 835–841.

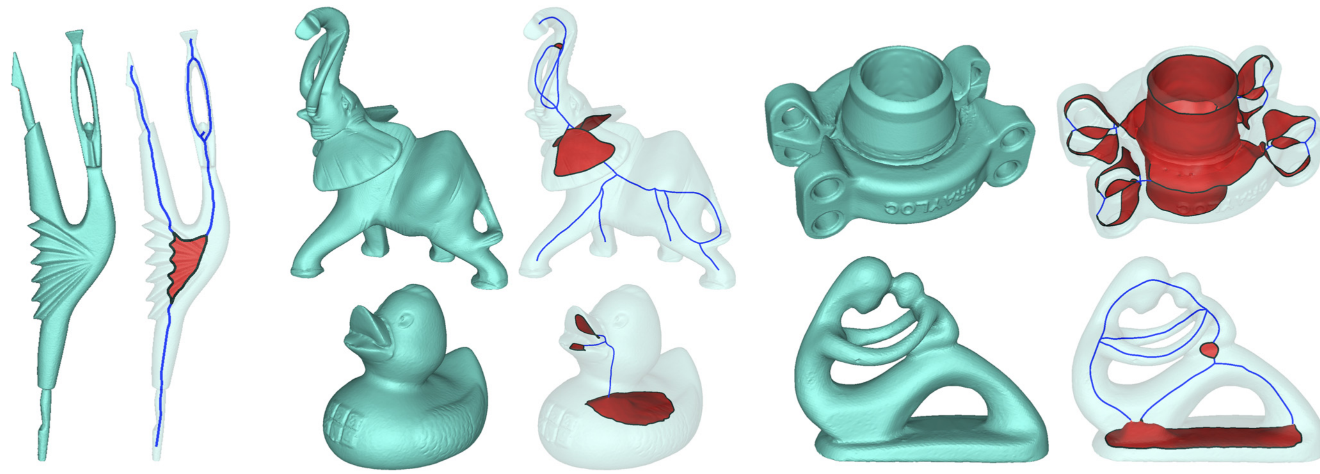

Figure 8: A gallery of models and their mixed-dimensional skeletons

Name	T-shape	Elephant	Fertility	Hand	Toy	Grayloc	Duck	Dancer	Bird	Fish		
Size (2^n)	6	7	7	7	7	7	7	8	8	8	9	10
Time(*s*)	0.67	2.17	2.64	2.72	4.91	6.42	13.94	2.33	2.63	51	419	3734
Mem (mb)	99.4	158.1	162.4	162.8	244.6	257.0	412.5	161.9	163.3	147.9	226.8	691.9

Figure 9: Time and memory performance for all models in the paper.

GOSWAMI, S., DEY, T. K., AND BAJAJ, C. L. 2006. Identifying flat and tubular regions of a shape by unstable manifolds. In *SPM '06: Proceedings of the 2006 ACM symposium on Solid and physical modeling*, ACM, New York, NY, USA, 27–37.

JU, T., BAKER, M. L., AND CHIU, W. 2007. Computing a family of skeletons of volumetric models for shape description. *Comput. Aided Des. 39*, 5, 352–360.

JU, T. 2004. Robust repair of polygonal models. *ACM Trans. Graph. 23*, 3, 888–895.

KATZ, S., AND TAL, A. 2003. Hierarchical mesh decomposition using fuzzy clustering and cuts. In *SIGGRAPH '03: ACM SIGGRAPH 2003 Papers*, ACM, New York, NY, USA, 954–961.

LAM, L., LEE, S.-W., AND SUEN, C. Y. 1992. Thinning methodologies-a comprehensive survey. *IEEE Trans. Pattern Anal. Mach. Intell. 14*, 9, 869–885.

MATVEEV, S. 2003. *Algorithmic Topology and Classification of 3-Manifolds*. Springer-Verlag Berlin.

OGNIEWICZ, R. L., AND KÜBLER, O. 1995. Hierarchic voronoi skeletons. *Pattern Recognition 28*, 3, 343–359.

PASCUCCI, V., SCORZELLI, G., BREMER, P.-T., AND MASCARENHAS, A. 2007. Robust on-line computation of reeb graphs: simplicity and speed. In *SIGGRAPH '07: ACM SIGGRAPH 2007 papers*, ACM, New York, NY, USA, 58.

PIZER, S. M., SIDDIQI, K., SZÉKELY, G., DAMON, J. N., AND ZUCKER, S. W. 2003. Multiscale medial loci and their properties. *Int. J. Comput. Vision 55*, 2-3, 155–179.

RENIERS, D., VAN WIJK, J., AND TELEA, A. 2008. Computing multiscale curve and surface skeletons of genus 0 shapes using a global importance measure. *IEEE Transactions on Visualization and Computer Graphics 14*, 2, 355–368.

ROSENFELD, A. 1979. Digital topology. *The American Mathematical Monthly 86*, 8, 621–630.

SHAKED, D., AND BRUCKSTEIN, A. M. 1998. Pruning medial axes. *Comput. Vis. Image Underst. 69*, 2, 156–169.

SHARF, A., LEWINER, T., SHAMIR, A., AND KOBBELT, L. 2007. On-the-fly curve-skeleton computation for 3d shapes. *Comput. Graph. Forum 26*, 3, 323–328.

SHERBROOKE, E. C., PATRIKALAKIS, N. M., AND BRISSON, E. 1996. An algorithm for the medial axis transform of 3d polyhedral solids. *IEEE Transactions on Visualization and Computer Graphics 2*, 1, 44–61.

SIDDIQI, K., AND PIZER, S. M. 2008. *Medial Representations*. Springer.

SIDDIQI, K., BOUIX, S., TANNENBAUM, A., AND ZUCKER, S. W. 2002. Hamilton-jacobi skeletons. *International Journal of Computer Vision 48*, 3 (July), 215–231.

SUD, A., FOSKEY, M., AND MANOCHA, D. 2005. Homotopy-preserving medial axis simplification. In *SPM '05: Proceedings of the 2005 ACM symposium on Solid and physical modeling*, ACM, New York, NY, USA, 39–50.

SVENSSON, S., NYSTRÖM, I., AND DI BAJA, G. S. 2002. Curve skeletonization of surface-like objects in 3d images guided by voxel classification. *Pattern Recognition Letters 23*, 12, 1419–1426.

TAGLIASACCHI, A., ZHANG, H., AND COHEN-OR, D. 2009. Curve skeleton extraction from incomplete point cloud. *ACM Transactions on Graphics, (Proceedings SIGGRAPH 2009) 28*, 3.

TSAO, Y. F., AND FU, K. S. 1981. A parallel thinning algorithm for 3-d pictures. *Comput. Graphics Image Process. 17*, 315–331.

ZHOU, Q.-Y., JU, T., AND HU, S.-M. 2007. Topology repair of solid models using skeletons. *IEEE Transactions on Visualization and Computer Graphics 13*, 4, 675–685.